Experimental and simulation investigation of n-heptane/ammonia dual fuel on a light-duty compression ignition engine

Cheng, Chong; Cordtz, Rasmus Faurskov; Førby, Niels Langballe; Schramm, Jesper

Published in:
International Journal of Hydrogen Energy

Link to article, DOI:
10.1016/j.ijhydene.2024.01.130

Publication date:
2024

Document Version
Publisher's PDF, also known as Version of record

International Journal of Hydrogen Energy 57 (2024) 1339–1353

Contents lists available at ScienceDirect

International Journal of Hydrogen Energy

journal homepage: www.elsevier.com/locate/he

Experimental and simulation investigation of n-heptane/ammonia dual fuel on a light-duty compression ignition engine

Chong Cheng [a,*], Rasmus Faurskov Cordtz [b], Niels Langballe Førby [a], Jesper Schramm [a]

[a] Technical University of Denmark, Copenhagen, Denmark
[b] Danish Technological Institute, Aarhus, Denmark

ARTICLE INFO

Handling Editor: Dr M Mahdi Najafpour

Keywords:
Ammonia fuel
Compression ignition engine
Heat release rate
Ignition delay
Multi-zones model
Flame propagation model

ABSTRACT

Ammonia is a carbon-free, promising fuel for hydrogen carriers. It is a liquid fuel under low-pressure conditions (8.62 bars) and can be easily stored. Many researchers have tried to apply it in engines because there are no carbon dioxide emissions when combusting it. However, ammonia is a low cetane number fuel and is difficult to ignite. It can be used in a dual fuel mode in compression ignition (CI) engines, i.e., a fuel such as diesel, n-heptane, dimethyl ether, hydrogen etc., is used as a pilot fuel to ignite the ammonia. In this work, n-heptane was used as the pilot fuel and ammonia was used as the primary fuel in a light-duty CI engine. The engine's heat release rate (HRR), cylinder pressure, ignition delay and indicated efficiency were investigated experimentally at 80 %, 89 %, 95 % and 98 % ammonia fuel energy proportion. In order to investigate the ignition and combustion characteristics of the dual fuel engine, a multi-zone combustion model for n-heptane and a flame propagation model for the ammonia fuel were developed. In this work, it is found that the combustion process of n-heptane/ammonia can be simulated in most cases by a multi-zone evaporative combustion model combined with a flame propagation model. This work also found that the ignition performance of n-heptane is more affected by the long chemical ignition delay. Eventually, it was found that the more minor the discrepancy between the simulated and experimental ignition delays, the more insignificant the discrepancy between the simulated heat release rates and cylinder pressures and the experimental ones. The HRR, cylinder pressure, physical and chemical ignition delays and indicated efficiency of the engine were then simulated. The simulation showed good agreement with experimental results for the 89 %, 95 % and 98 % ammonia fuel energy proportion cases. The simulated physical ignition delay was 1.45–2.37 CA deg, the chemical ignition delay was 7.21–8.88 CA deg, and the indicated efficiency was 39.84%–42.80 % (for the three cases with 89 %, 95 % and 98 % ammonia fuel energy proportions). A detailed analysis of each parameter was conducted.

1. Introduction

To date, ships in maritime transportation and most vehicles are powered by fossil fuels such as petrol and diesel, which produce large amounts of greenhouse gases such as carbon dioxide [1,2]. Carbon dioxide is a strong driver of the greenhouse effect, causing an increase in the earth's surface temperature, raising sea levels, acidifying the oceans and leading to drought and desertification of the land [3,4]. The reduction of carbon dioxide and other greenhouse gases is therefore of great importance. The European Union was the first major economy to declare its contribution to the targeted reduction of greenhouse gases in the agreement, i.e., a 40 % reduction of domestic greenhouse gases by 2030 compared to 1990 [5,6]. In the field of internal combustion engines (ICE), the use of carbon-free fuels such as ammonia and hydrogen fuels, therefore, becomes particularly relevant, as there are no CO2 emissions. Ammonia fuel is one of the most produced chemicals in the world and can be produced in a power-to-X process [6]. One of the main production methods is the Haber-Bosch process, in which hydrogen and nitrogen are reacted with an iron-based catalyst at high pressure (300 bar) and temperature (673 K) to produce ammonia fuel [1]. Ammonia fuel has some difficulties in ICE applications. For example, ammonia fuel is difficult to ignite, and the minimum ignition energy (680 mJ) is much higher than that of diesel, gasoline, methanol, and ethanol fuels [7]. The low flame speed of ammonia and its corrosiveness to engines also limit the use of this fuel. In this work, n-heptane was used as the pilot fuel and ammonia as the primary fuel in a CI

* Corresponding author.
E-mail addresses: cchen@dtu.dk (C. Cheng), rfc@teknologisk.dk (R.F. Cordtz), nilfor@dtu.dk (N.L. Førby), jessc@dtu.dk (J. Schramm).

https://doi.org/10.1016/j.ijhydene.2024.01.130
Received 30 October 2023; Received in revised form 2 January 2024; Accepted 10 January 2024

engine.

In order to investigate the ignition and combustion processes of n-heptane and ammonia fuels in engines, combustion modelling is essential. Stiesch [8] developed a new multi-zone phenomenological combustion model for a diesel engine, including spray dispersion, droplet heating and evaporation, droplet and air mixing, ignition delay, and a final combustion sub model. Stiesch then selected two engine operating conditions for the simulation. The first operation condition was with an engine speed of 1500 rpm and a mean effective pressure of 980 kPa, and the second was with an engine speed of 1500 rpm and a mean effective pressure of 2220 kPa. The simulations were in good agreement with the experimental results in terms of engine HRR and cylinder pressure and thus demonstrated the validity of the multi-zone combustion model. Papagiannakis [9] has developed a two-zone combustion model with diesel as the pilot fuel and natural gas as the primary fuel. The volume change and the amount of fuel entrained were calculated in the pilot fuel zone. The flame propagation rate of natural gas zone and the amount of fuel burned were calculated. The authors conducted experiments on a single cylinder four-stroke dual fuel engine at 2000 rpm, 20 %, 40 %, 60 % and 80 % load. The simulated HRR and cylinder pressures are in good agreement with the experimental data, and the results were analyzed. In addition, the duration of combustion, ignition delay and engine efficiency were simulated and analyzed. Nadimi [10] has developed a two-zone 1D ammonia/diesel dual fuel engine combustion model by applying the target pressure method using AVL BOOST software. The model was built with different internal energies, volume changes etc., in the two zones. The heat loss, enthalpy transfer and blow-by loss were calculated using BOOST software. The ammonia/diesel dual fuel's combustion characteristics were analyzed using this model. In addition, an experimental study of the ammonia/-diesel dual fuel engine was carried out. The authors varied the λ value from 1.34 to 1.52 for different energy proportions of ammonia and diesel fuel (ammonia-diesel energy proportions from 14.9 % to 84.16 %). A detailed analysis of the indicated thermal efficiency, exhaust temperature, cylinder pressure, and HRR was conducted. The results showed that the highest ammonia energy proportion was 84.16 %, and the highest indicated thermal efficiency was 37.1 %. There is a paucity of published literature on the modelling of combustion in dual-fuel ammonia engines. The above literature, including ammonia, diesel, and natural gas fuel in engine applications, is highly inspiring for the n-heptane multi-zone modelling and the ammonia flame propagation modelling in this work.

Experimental research on ammonia-fuelled engines is also vital, as the combustion characteristics of the engine can be directly investigated, and, in addition, experimental data can be applied to calibrate the model of combustion. Yousefi [11] investigated the effect of diesel split injection (two-pulse diesel injection) on the combustion and emissions of ammonia/diesel dual-fuel engines. HRR and cylinder pressure were studied and analyzed for six cases of diesel split ratio ranging from 0 % to 45 %. The indicated thermal efficiency of the engine, CA50, CA10-90 and N_2O emissions were discussed. The experiments showed that applying the diesel split injection mode increases the indicated thermal efficiency to 39.72 %, which is higher than the diesel-only combustion mode (38.62 %). At the optimum operating point, i.e., 40 % diesel split ratio (−57 ATDC for the first injection and −16 ATDC for the second), CO_2 emissions were reduced by 23.7 % and the indicated thermal efficiency was increased by 2 % (compared to the diesel-only operating mode). Mi [12] has studied diesel as a pilot fuel and ammonia as a primary fuel in a compression-ignition engine with 40 %, 50 %, 60 % and 70 % ammonia fuel energy fraction. Cylinder pressure and HRR were investigated for the engine with injection timings of −10, −15 and −20 CA ATDC. The engine's NO_X, CO and NH_3 emissions results were analyzed and discussed. The results indicated that the pilot injection strategy was able to reduce ammonia emissions from 1000 ppm to 8000 ppm, and this strategy could achieve a high indicated thermal efficiency of 45 %. Førby [13] conducted a combustion characteristics and emissions study on a light-duty CI engine using n-heptane as the pilot fuel and ammonia as the primary fuel. Førby investigated HRR, ignition delay, coefficient of variation (COV) and NO emissions at 78 %, 80 %, 89 %, 95 % and 98 % ammonia fuel energy proportions with an λ of 1.1. It was found that the ignition delay tended to increase with increasing ammonia fuel energy proportion, ranging from 8.51 to 10.02 deg. The highest indicated efficiency was 37.21 %. The combustion efficiency gradually increased with the increasing proportion of ammonia fuel. Frigo [14] conducted ammonia-hydrogen fuel research on a 2-cylinder spark ignition (SI) engine with a displacement volume of 505 cm^3. The engine used hydrogen fuel as a combustion promoter, which effectively improved the ignition performance and the combustion velocity of the ammonia fuel. The net heat release of gasoline and ammonia-hydrogen fuels was compared at 4000 rpm with λ maintained at 1. The peak of the net heat release of ammonia-hydrogen fuel appeared later than that of gasoline. The NOx emission concentration of ammonia-hydrogen fuel was low, 1700 ppm at full load. The COV was below 10 % in the cases with various hydrogen/ammonia fuel energy ratios. Ryu [15] investigated the combustion of ammonia and hydrogen fuels in a four-stroke SI engine with a compression ratio of 10:1 at 1800 rpm. The hydrogen fuel was derived from the dissociation catalysis of ammonia fuel. The addition of hydrogen fuel increased the engine power while decreasing the exhaust temperature of the engine at various ammonia fuel injection durations (10–23 ms). The exhaust temperature of the cases where hydrogen fuel was added was about 780° Celsius and 820° Celsius without hydrogen fuel. The cylinder pressure of the hydrogen-fuelled case is also higher than the cylinder pressure of the non-hydrogen-fuelled case. Brake-specific NH_3 emissions were significantly lower in the ammonia case with hydrogen addition, about 0.4 g/kWh, compared to about 2.8 g/kWh in the case without hydrogen addition, thus demonstrating the feasibility of ammonia-hydrogen fuel combustion in the engine as well as the excellent emission characteristics.

There is considerable previous experimental research on the dual fuel of ammonia with other fuels in CI engines and some in SI engines [16–18]. Few research studies have been on modelling ammonia with other fuels in CI engines. In the present work, ammonia fuel with different energy proportions and n-heptane has been investigated using a light-duty BUKH engine as experimental equipment. The experimental HRR and cylinder pressure, ignition delay, and indicated efficiency were investigated in detail. A multi-zone model for n-heptane and a flame propagation model for ammonia were established. The multi-zone model was calibrated and validated for n-heptane fuels. The HRR, cylinder pressure, physical and chemical ignition delays and indicated efficiency were simulated and analyzed for deviations.

2. Experimental setup

The engine used for the experiments is a modified dual-fuel BUKH DV24 ME engine. The pilot fuel is n-heptane, and the primary fuel is ammonia. N-heptane burns first to ignite the ammonia fuel. N-heptane is chosen as pilot fuel mainly because of its low viscosity (0.57 mm^2/s) [13, 19] and high cetane number (53–56) [20]. The lower viscosity results in a faster evaporation process, which shortens the physical ignition delay. A higher cetane number shortens the overall ignition delay and improves ignition performance. Although n-heptane produces some pollutants during combustion, this work took n-heptane as pilot fuel (minor energy ratio). Therefore, the pollutant's impact is not significant [21, 22]. N-heptane is injected into the cylinder via a piezo-electric Siemens gasoline direct injection (GDI) injector, which shortens the droplet break-up time and thus facilitates n-heptane ignition. However, n-heptane is a non-renewable fuel, so in the long term, it should be replaced with renewable fuel, thus ensuring that all energies are renewable. The gaseous ammonia fuel is aspirated into the intake manifold driven by the vapor pressure of the tank.

The schematic diagram of this engine is illustrated in Fig. 1. It consists of two cylinders, one of which is a modified dual fuel (n-heptane and ammonia) cylinder and the other is the original diesel fuel cylinder. The power of the diesel cylinder ensures stable engine start-up and operation. In the dual fuel cylinder, a Kistler piezo-electric pressure transducer collects pressure data, which is measured ten times at each crank angle degree. A ceramic air heater heats the intake air, and the intake air is pressurized by an external air compressor simultaneously. Two air flow meters measure the mass flow rate of the ambient and heated intake air, respectively. The n-heptane tank is pressurized using a nitrogen pressure vessel to ensure an injection pressure of 120 bars. A Coriolis mass flow meter is used to measure the consumption of n-heptane. The pressure transducer measures the average cylinder pressure over 50 consecutive cylinder cycles, and these data are used to calculate the HRR. The photos of the engine are presented in Fig. 2. Table 1 specifies the engine parameters.

3. Simulation model

3.1. Model description

The model is a phenomenological model of dual fuel combustion (n-heptane and ammonia), where pilot fuel (n-heptane) is modelled employing a multi-zone model. The multi-zone model was first proposed by scholars such as Hiroyasu and Kadota [23,24]. The multi-zone model has since been applied and further developed by various scholars such as Bazari, Gao, and Kouremenos [25–27]. It is accurate for predicting the combustion of CI engines. The n-heptane in the multi-zone model undergoes fuel break-up, atomization, evaporation, mixing, ignition delay, and combustion heat release processes. The multi-zone model also includes a portion of ammonia fuel entrainment, but the ammonia fuel combustion is mainly from the flame propagation model. When the n-heptane starts to combust, the ammonia fuel is ignited simultaneously. At this point, the laminar flame velocity of the ammonia fuel needs to be calculated. After that, the turbulent flame speed is calculated based on engine parameters such as engine piston speed and compression ratio. The mass of the ammonia fuel burning in the cylinder can be further determined from the turbulent flame speed. The multi-zone model, together with the flame propagation model, enables the calculation of the overall HRR, cylinder pressure, physical and chemical ignition delay, engine efficiency etc.

As illustrated in Fig. 3, the multi-zone model of n-heptane comprises a number of zones of different colors. These zones are marked horizontally and vertically by j and k, respectively. The zones are divided into concentric circular structures. At the time when the n-heptane is first injected, the zones are shown in grey in Fig. 3. These zones contain only the n-heptane in its liquid state. After that, the n-heptane breaks up and becomes fine droplets, which causes a dramatic increase in resistance and a sharp decrease in velocity in the zones of motion. At this point, the air in the unburned zone (assuming that the mixture entrained is air) is entrained into the different zones according to the conservation of momentum. So these blue zones include both air and droplets. After the break-up, the droplets evaporate immediately, so the green zones in the next stage include air, droplets, and evaporated fuel vapor. As evaporation proceeds, the yellow zone consists of more and more of the concentrated mixture. When the red zones' temperature, pressure and fuel-to-air equivalence ratio meet certain conditions, combustion begins. The dark yellow zones after combustion comprise the post-combustion pollutant and the remaining air or n-heptane. There is no exchange of mass or energy between the various zones [8,28]. The reason for assuming that there is no exchange of mass and heat between the zones was because, ultimately, in order to model the heat release rate and cylinder pressure of the whole cylinder. The exchange of mass and heat within the zones does not significantly affect the modelling of the parameters of the cylinder as a whole, which is equivalent to the internal flow of mass and heat. However, after assuming no mass and heat exchange, droplet break-up, air entrainment, evaporation, and combustion within the zones can be modelled more conveniently and relatively accurately. The heat exchange between the zones and the cylinder wall has a more significant impact on the simulation of the heat release rate and cylinder pressure, so the heat exchange between the zone and the cylinder wall is considered here. After the n-heptane has started to combust, the pre-mixed ammonia fuel in the cylinder is ignited. The turbulent flame of the ammonia fuel begins to propagate through the cylinder along the conical spray area. The propagating flame will sweep through the volume of the cylinder. The flame propagation speed and the ammonia mixture's density determine the mass of ammonia fuel burned. The blue arrow in Fig. 3 shows the propagation's exact direction.

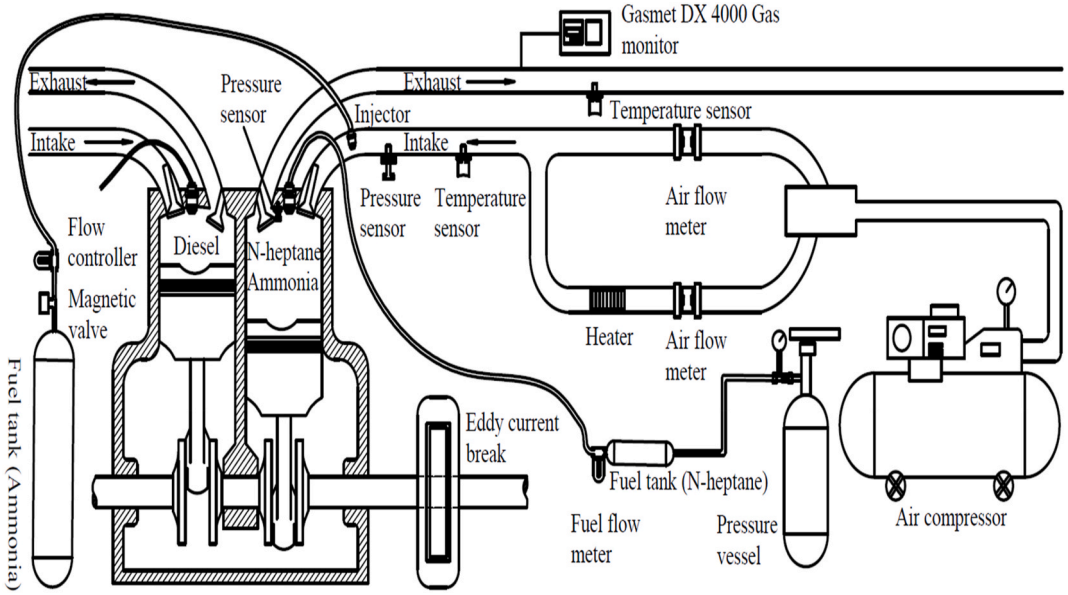

Fig. 1. Schematic diagram of the experimental dual-fuel engine set-up.

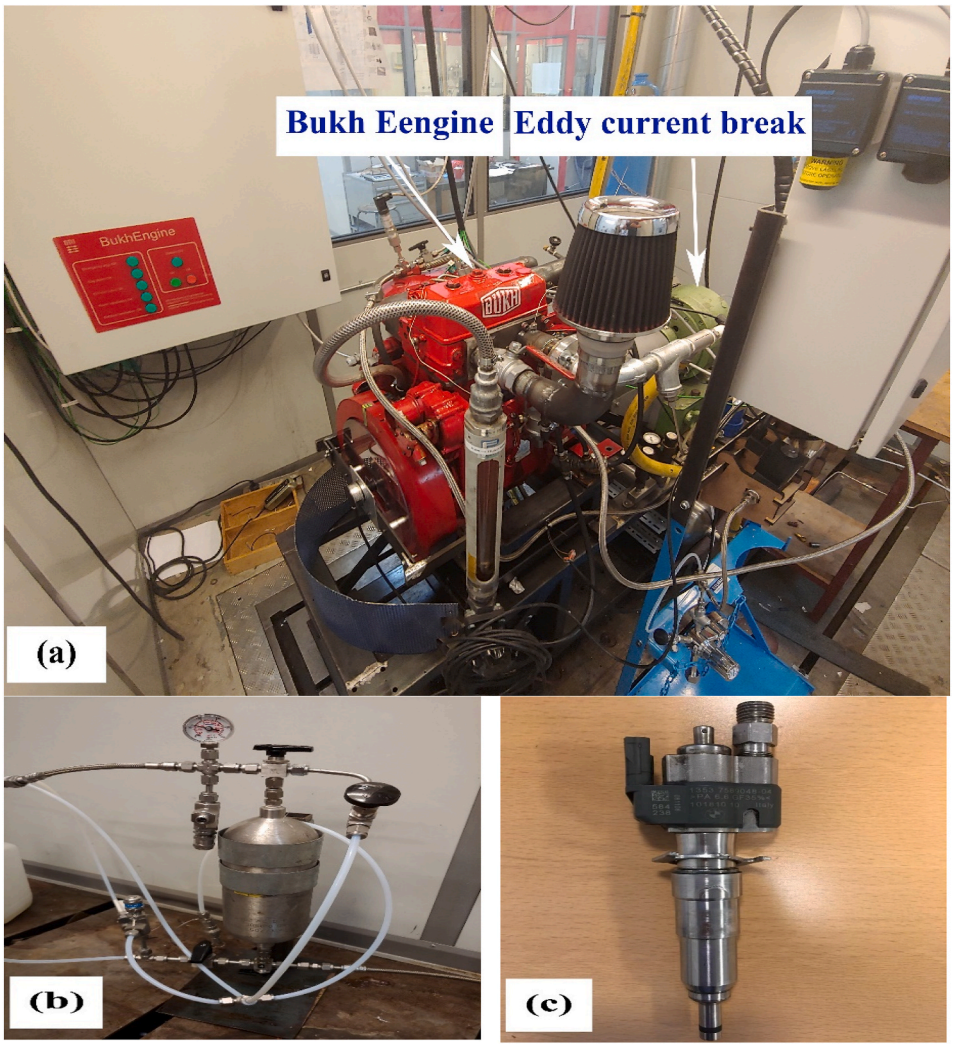

Fig. 2. Photographs of the Bukh engine experimental setup: (a) engine main part; (b) pressurized fuel tank; (c) Siemens direct injection GDI fuel injector.

Table 1
BUKH DV24 ME specifications.

Engine parameter	Numerical value
Rated power	17.6 [kW]
No. of cylinders	2 [-]
Bore diameter (B)	85 [mm]
Stroke (S)	85 [mm]
Connection rod length (L)	160 [mm]
Geometric compression ratio[a] (CR_g)	18 [-]
Effective compression ratio[b] (CR_e)	16.4 [-]
Displacement Volume (V_d)	964 [cc]
Intake valve close (θ_{close})	139 [CAD BTDC]
Exhaust valve open (θ_{open})	126 [CAD ATDC]
Engine speed (in this work)	1200 [rpm]
Piezo-electric injector type	Siemens GDI injector
Injector equivalent diameter	0.34 [mm]
Injector injection pressure	120 [bar]

[a] Ideally designed compression ratio.
[b] Compression ratio at which the engine is actually running (such as considering the effects of valve timing and boosting).

3.2. Pilot fuel injection and ammonia entrainment

Once the pilot fuel (n-heptane) has been injected into the cylinder, the parameters relating to the physical size of its spray are critical. This physical size determines the burning rate of the ammonia fuel involved in the burn zone. The first parameter to be introduced here is the initial spray cone angle [9,27].

$$\theta = \left(\frac{d_{inj}^2 \bullet \rho_u \bullet \Delta p}{\mu_u} \right)^{0.25} \tag{1}$$

The pilot fuel of the spray is considered to be steady and consists of a number of zones. Here, the spray penetration length is given by the following equation [23,29].

$$S = 2.95 \bullet \left(\frac{\Delta p_{inj}}{\rho_u} \right)^{0.25} \bullet \sqrt{d_{inj} \bullet t} \tag{2}$$

After the pilot fuel has been injected into the cylinder, a spray is formed, which is called the "burning zone". Since the spray has a certain speed, the volume of the spray changes over time. As a result of this volume change, the ammonia fuel mixture from other areas of the cylinder is drawn into the burning zone. But at the same time, this burning zone also contains the pilot fuel that was first injected. The evaporation of pilot fuel will be described in more detail in the following section. The volume change of the burning zone is expressed as follows.

$$\frac{dV_b}{dt} = \frac{\pi}{3} \bullet tan^2\,\theta \bullet \frac{dS}{dt} \tag{3}$$

Because the burning zone is continuously expanding and moving, the mass of the entrained ammonia fuel can be expressed as the change in volume multiplied by the density of the ammonia zone gaseous fuel, as shown in Eq. (4).

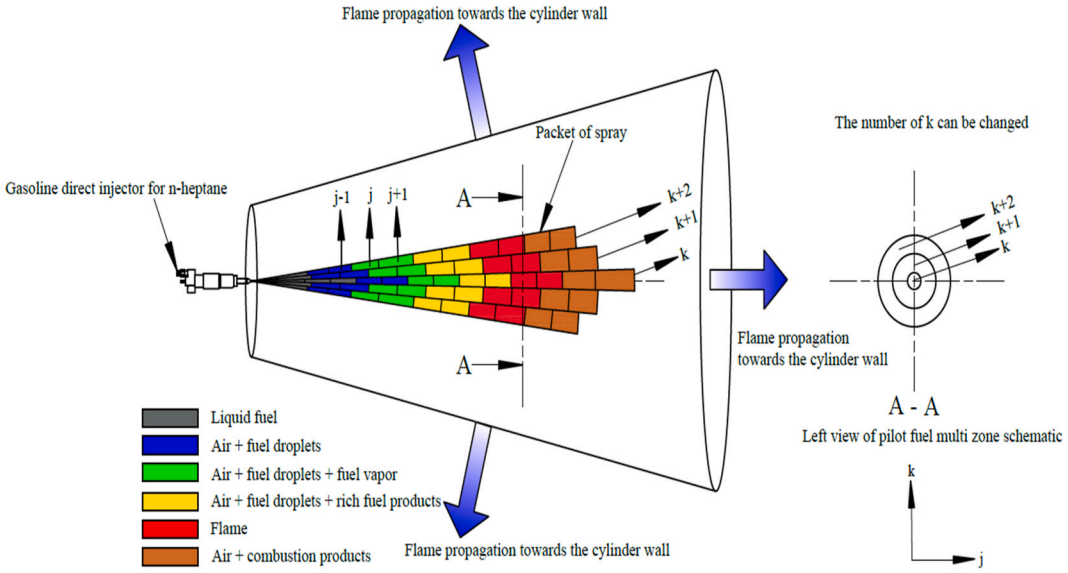

Fig. 3. Axisymmetric illustration of the n-heptane multi-zone model and the flame propagation model of ammonia fuel.

$$\frac{dm_b}{dt} = \rho_{am} \bullet \frac{dV_b}{dt} \tag{4}$$

3.3. Pilot fuel break-up and fuel air mixing

For the process of break-up and evaporation of n-heptane pilot fuel, a multi-zone model is used here for the simulation. The burning zone described above is divided into different concentric circular zones, where the fuel breaks up after a short time when the n-heptane is injected. The moment of break-up is when the pilot fuel starts to evaporate. Here the time of break-up varies depending on the zones. The most peripheral zones have a high air resistance because of the large contact area with the ammonia mixture in the cylinder, so the break-up time is relatively short. The introduction of the parameter k in the break-up time equation below results in different break-up times for different zones.

$$t_{bu(j,k)} = 28.65 \frac{\rho_f \bullet d_{noz}}{\sqrt{\rho_{SOI}(p_{inj} - p_{SOI})}} \frac{(k_{max} + 1) - k}{k_{max}} \tag{5}$$

The speed of the spray varies considerably before and after the n-heptane fuel is broken-up. Before the break-up, the fuel velocity is fast. After the break-up, however, the air resistance increases instantly because the fuel becomes fine droplets. As a result, the velocity decreases sharply. Especially in the zones at the periphery of the spray, the velocity decreases more rapidly because of the greater resistance in all zones. N-heptane velocities before and after break-up are expressed as follows [28,30].

$$v_{inj} = 0.6 \bullet \sqrt{\frac{2(p_{inj} - p_{SOI})}{\rho_f}} \tag{6}$$

$$v_{(j,k)} = 1.48 \left(\frac{(p_{inj} - p_{SOI}) {d_{noz}}^2}{\rho_{SOI}} \right)^{\frac{1}{4}} \bullet \frac{1}{\sqrt{t}} \bullet e^{\left(-3.86 \bullet 10^{-2} \bullet (k-1)^2\right)} \tag{7}$$

At the moment the n-heptane breaks up, the velocity of the zones decreases dramatically. Therefore, according to the principle of conservation of momentum, the air is instantly entrained into the zones because of the reduced velocity (it is assumed that the entrained mixture is air, as the pilot fuel has relatively less mass, so the small amount of entrained mixture is assumed to be air at this point).

$$m_{0(j,k)} = c_0 \frac{v_{inj}\, m_{f(j,k)}}{v_{0(j,k)}} \tag{8}$$

After the n-heptane breaks up, the air is also continuously entrained into the zones. The exact amount of air entrainment is calculated as shown in Eq. (9). c_0 and c_{mix} may be required for calibrated of any engine.

$$\dot{m}_{entr(j,k)} = \frac{\dot{m}_{f(j,k)} v_{inj} - c_{mix} m_{j,k} \dot{v}_{j,k}}{v_{j,k}} \tag{9}$$

3.4. Evaporation of pilot fuel

The evaporation process of pilot fuel determines the process of its combustion and the ignition delay. This is because the ignition delay is directly related to the air-fuel equivalent ratio in the zones. The air-fuel equivalent ratio is directly related to the amount of pilot fuel evaporated. Before the droplet evaporation, the Sauter Mean Diameter (SMD) of the fuel after the break-up needs to be determined. After that, the droplet temperature rate of change, the convective heat transfer rate of change and the mass rate of change are calculated. The evaporation process is based on the Borman and Johnson model [31].

$$D_{0(j,k)} = 23.9 \bullet 10^{-6} \Delta p_{inj}^{-0.135} \rho_a^{0.12} B^{0.131} \tag{10}$$

$$\dot{T}_{d(j,k)} = \frac{1}{m_{d(j,k)} c_{p,f}} \left(\dot{Q}_{d,(j,k)} + \dot{m}_{d,(j,k)} \Delta h_{evap} \right) \tag{11}$$

$$\dot{Q}_{d(j,k)} = \pi \bullet D_{0(j,k)} \bullet k_{s(j,k)} \bullet \left(T_{g(j,k)} - \dot{T}_{d(j,k)} \right) \bullet \frac{z}{e^z - 1} \bullet Nu_{(j,k)} \tag{12}$$

$$\dot{m}_{d,(j,k)} = -\pi \bullet D_{0(j,k)} \bullet D_{AB} \bullet \rho_{s(j,k)} \bullet \ln\left(\frac{p_{cyl}}{p_{cyl} - p_{v(j,k)}} \right) \bullet Sh_{(j,k)} \tag{13}$$

When modelling the evaporation of n-heptane droplets, some specific formulas and the thermal properties of the droplets are involved. These detailed formulas affect the entire evaporation process. Table 2 presents this specific information.

3.5. Ignition delay

Ignition delays include physical ignition delay and chemical ignition delay. Physical ignition delay refers to the process of fuel breaking up, atomization, evaporation and mixing with air. Chemical ignition delay

Table 2
Parameters of thermodynamic properties for droplet modelling.

	n-Heptane	Unit
Δh_{evap}	319.7	[kJ/kg]
p_v	$ln\, P_v = 12.12767 - \frac{6738.9067}{(T-167.44)}$	[Pa]
D_{AB}	0.0000014	[m^2/s]
$c_{p,f}$	1980	[J/(kg • K)]
Nu	$Nu = 2 + 0.6Re^{1/2}\, Pr^{1/3}$	[−]
Sh	$Sh = 2 + 0.6Re^{1/2}Sc^{1/3}$	[−]
Re	$Re = \frac{0.3\rho v D}{\mu}$	[−]
Pr	$Pr = \frac{C_p \mu}{k}$	[−]
Sc	$Sc = \frac{\mu}{\rho \bullet DB}$	[−]
z	$z = \frac{c_{p,v} \bullet \dot{m}_{f,v}}{\pi \bullet D \bullet k_s \bullet Nu}$	[−]
ρ_s	$\rho_s = \frac{\left(\frac{p_{cyl}}{R_{FP}T_{FP}} + \frac{p_v}{R_f T_f}\right)}{2}$	[kg/m^3]

refers to the period between the chemical decomposition of n-heptane and the rapid chemical reaction leading to combustion. In this section, we focus on chemical ignition delay. The chemical ignition delay is predicted using a semi-empirical formula. Then, the ignition delay is calculated based on the transient temperature, pressure, and n-heptane air equivalent ratio in the cylinder. The effect of entrainment of ammonia mixture into n-heptane is taken into account when calculating ignition delay, as ignition delay is more sensitive to ammonia fuel.

Ignition delay can significantly affect the combustion process. If the ignition delay is long, a large amount of n-heptane gas will accumulate during the ignition delay, resulting in a large share of the premixed combustion phase and a small share of the mixing-controlled combustion phase. Conversely, if the ignition delay is short, there will be a small share of the premixed combustion phase and a large share of the mixing-controlled combustion phase.

Ignition delay is an essential parameter in engine operation. Because it affects the type of combustion, which in turn affects the cylinder pressure, it also significantly impacts engine emissions. The ignition delay is given in Eq. (14).

$$\tau_{id(j,k)} = A\left(\frac{p}{p_{ref}}\right)^{-\kappa} \varnothing_{(j,k)}{}^{-\beta} \exp\left(\frac{E_t}{T_{(j,k)}}\right) \tag{14}$$

The cylinder's temperature, pressure and fuel-air equivalent ratio are varied in real-time. In order to express the effect of this varied real-time variable on the ignition delay, the inverse of Eq. (14) is integrated. When the result of the integration is greater than or equal to 1, then combustion begins. This is shown in Eq. (15).

$$\int_0^{\tau_{id}} \frac{1}{\tau_{id(j,k)}} dt = 1 \tag{15}$$

3.6. Flame propagation

After the n-heptane combusts, it is assumed that a flame is generated simultaneously on the outer side of the entire conical region of the pilot fuel. This flame will propagate in a direction perpendicular to the outer surface of this region. The propagation direction is shown by the blue arrow in Fig. 3. The flame propagation sweeps through a certain volume, and the swept volume multiplied by the density of the ammonia fuel is the mass of the ammonia fuel burned due to the flame propagation. In practice, the flame thickness of the laminar flame is about 0.2 mm, but this thickness is much less compared to the dimensions of the cylinder, so it is negligible here [32]. The velocity of the laminar flame is directly related to the fuel-air equivalent ratio of the ammonia fuel, the cylinder temperature, and the cylinder pressure. Here, the flame velocity is considered only for the flame velocity of the ammonia fuel and is not added to the conical area movement velocity of the pilot fuel. The laminar flame velocity is calculated with respect to the flame reference velocity, temperature, and pressure exponents [33]. The reference velocity calculation is based on the maximum combustion velocity at the reference temperature and pressure and the fuel-air equivalent ratio. The temperature and pressure exponents, on the other hand, are calculated independently of the fuel type. The specific laminar flame velocity calculation process is described in Eqs. (16)–(18) [33,34].

$$v_l = v_{ref}\left(T_u/T_{ref}\right)^{\alpha}\left(p_u/p_{ref}\right)^{\gamma} \tag{16}$$

$$v_{ref} = v_{ref,max} + s_1(\varnothing - 1.1)^2 + s_2(\varnothing - 1.1)^3 \tag{17}$$

$$\alpha = 2.18 - 0.8(\varnothing - 1) \tag{18}$$

$$\gamma = -0.16 + 0.22(\varnothing - 1) \tag{19}$$

The combustion process of an engine is turbulent. In expressing turbulence, a flame coefficient of turbulence is required, which is related to the compression ratio of the engine, the engine speed, and the density of the burned and ammonia zones in the cylinder, among other factors. This coefficient is the ratio of the turbulent combustion velocity to the laminar combustion velocity. This is expressed in Eq. (20) [35–37].

$$f_f = \frac{v_t}{v_l} = 1 + \left(\frac{CR}{8}\right)^{a}\left(\frac{\rho_{am}}{\rho_b}\right)^{\frac{1}{2}}\left(0.5\frac{\overline{v}_P}{v_l}\right)^{\frac{1}{2}}\left(1 - \exp\left(-\frac{R_f}{cB_{cyl}}\right)\right) \tag{20}$$

The turbulent flame propagates perpendicular to the conical jet zone and will sweep over the zone inside the cylinder. The change in swept area multiplied by the speed of the turbulent flame is the change in swept volume. The change in swept volume multiplied by the density of the ammonia fuel is the mass of the ammonia fuel burned. This is shown in Eqs. (21) and (22) [38].

$$\frac{dV_{b,fl}}{dt} = v_t \bullet \frac{dA}{dt} \tag{21}$$

$$\frac{dm_{b,fl}}{dt} = \rho_{am} \bullet \frac{dV_{b,fl}}{dt} \tag{22}$$

3.7. Temperature in the different zones

The zones of the cylinder include multiple zones of pilot fuel and ammonia fuel zone. The temperature of the pilot fuel zones affects the ignition delay and the evaporation of the n-heptane. This, in turn, has a significant impact on the subsequent combustion. After ignition, the zone temperature influences the heat transfer from the different zones to the cylinder wall, piston top and cylinder head. The temperature of the ammonia fuel zone is used to calculate the heat transfer in this zone and to provide inputs for later ammonia pollutant modelling. The energy conservation law and the ideal gas law are used to derive the zone temperatures. The specific temperature equations are shown in Eqs. (23) and (24).

$$\dot{T}_{(j,k)} = \frac{-\dot{Q}_{d(j,k)} + \dot{m}_{evap(j,k)}h_{sat} + \dot{Q}_{HR(j,k)} + \dot{m}_{entr(j,k)}h_a - \dot{Q}_{loss(j,k)} - \dot{m}_{(j,k)}h_{(j,k)} + V_{(j,k)}\dot{p}}{m_{(j,k)}\left(c_{v,(j,k)} + R_{BP(j,k)}\right)} \tag{23}$$

$$\dot{T}_{am} = \frac{\sum \dot{m}_{entr,SP}(u_{am} - h_{am}) - \dot{Q}_{loss,am} - RT_{am}\dot{n}_{am} + V_{am}\dot{p}}{\left(m_{am}c_{v,am} + Rn_{am}\right)} \tag{24}$$

3.8. Heat transfer model

Woschni correlation is a heat transfer model that is now widely used and considered relatively accurate. The heat transfer part here involves the cylinder wall, the cylinder head and the top of the piston, each part of which is calculated separately. The heat transfer zones in the cylinder

include the multi-zones of pilot fuel and the ammonia-fuel zone. The calculation of the area of the different heat transfer parts and the calculation of the heat transfer coefficient in the Woschni formula are expressed in the following equations and Table 3.

$$\dot{Q}_{loss} = \sum_{1}^{N} A_i h_w \left(T_g - T_{wall,i}\right) \tag{25}$$

$$h_w = 0.00326 \bullet B_{cyl}^{-0.2} \bullet p^{0.8} \bullet T^{-0.55} \bullet w^{0.8} \tag{26}$$

$$\dot{Q}_{loss(j,k)} = \dot{Q}_{loss} \frac{m_{(j,k)} T_{(j,k)}}{\sum m_{(j,k)} T_{(j,k)}} \tag{27}$$

3.9. Calculation of HRR and cylinder pressure

The HRR is a highly significant parameter of an engine, which affects the engine's combustion type. The type of combustion further influences the efficiency and emissions [39]. The HRR is additionally used to calculate the cylinder pressure. When calculating the HRR, there are four parts. The first two parts are the heat released from the combustion of n-heptane, including the premixed and diffusion combustion parts. The third part is the expanding area of the n-heptane spray, which will continuously entrain a portion of the ammonia fuel into the expanded n-heptane spray area, which will be combusted after the n-heptane fuel is ignited. The fourth part is because of pilot-fuel combustion. The ammonia fuel is ignited. The flame propagation of the ignited ammonia fuel sweeps through the ammonia fuel mixture, which in turn, releases the heat of the ammonia fuel. This makes up the last part of the HRR.

The amount of fuel combusted during premixed and diffusion combustion of n-heptane is calculated according to the following rules. During the current simulation time step of the zone, if there is enough air in the zone to burn the fuel (calculated from the air-fuel equivalent ratio), then all evaporated fuel will be burned. If there is an excess of evaporated fuel in the zone, then the amount of fuel to be burned is calculated based on the amount of air available at that time, and the amount of fuel is limited by the amount of air available. Furthermore, a trigonometric function is used to hamper the HRR at the beginning and end of the combustion process [40]. This is shown in Eqs. (28) and (29).

$$\dot{Q}_{HR,p(j,k)} = y \bullet LHV_n \bullet \boldsymbol{min}\left(\frac{m_{v,SOC(j,k)}}{\Delta t_p}, \frac{m_{a,SOC(j,k)} / AF_{stoic}}{\Delta t_p}\right) \tag{28}$$

$$y = \frac{\pi}{2\Delta\theta} \sin\left(\pi \frac{\theta - \theta_0}{\Delta\theta}\right) \tag{29}$$

In the diffusion-controlled combustion calculation, diffusion combustion is assumed to occur concurrently with premixed combustion. The fuel vapor amount and droplet evaporation rate during diffusion combustion are intimately related. During diffusion combustion, the amount of n-heptane vapor and air in the zone are shown in Eqs. (30) and (31).

$$m_{v,diff(j,k)}(t) = m_{v(j,k)}(t) - m_{v,p(j,k)}(t) - m_{v,diff,con(j,k)}(t) \tag{30}$$

$$m_{a,diff(j,k)}(t) = m_{a(j,k)}(t) - m_{a,p(j,k)}(t) - m_{v,diff,con(j,k)}(t) \bullet AF_{stoic} \tag{31}$$

Therefore, the HRR for the diffusion part of the combustion can be calculated using Eq. (32).

Table 3
Area calculation and temperature estimation for different heat transfer components.

	Area (A_i)	Temperature (T_i)
Cylinder head	$A_1 = \frac{\pi}{4} {B_{cyl}}^2$	$T_1 = 500$ °C
Piston top	$A_2 = A_1$	$T_2 = 300$ °C
Cylinder liner	$A_3 = x(\theta)\pi B_{cyl}$	$T_3 = 100$ °C

$$\dot{Q}_{HR,diff(j,k)} = y \bullet LHV_n \bullet \boldsymbol{min}\left(\frac{m_{v,diff(j,k)}(t)}{\Delta t_{diff}}, \frac{m_{a,diff(j,k)}(t) / AF_{stoic}}{\Delta t_{diff}}\right) \tag{32}$$

The total of four parts of HRR is calculated as shown in Eq. (33).

$$\dot{Q}_{HRR} = \sum_{1}^{j \bullet k} \left(\dot{Q}_{HR,p(j,k)} + \dot{Q}_{HR,diff(j,k)}\right) + LHV_{ammo} \bullet \left(\frac{dm_b}{dt} + \frac{dm_{b,fl}}{dt}\right) \tag{33}$$

Once the HRR has been determined, the rate of change of cylinder pressure can be calculated. When calculating the rate of change of cylinder pressure, it is assumed that the pressure in all cylinder zones is uniform [23]. The heat losses are calculated using the Woschni formula described earlier. The specific heat parameters are obtained using the instantaneous average cylinder temperature from the Cantera software. The cylinder pressure is given in Eq. (34).

$$\dot{p} = \frac{\left(\frac{c_p}{c_v} - 1\right)}{V_{cyl}} \left(\dot{Q}_{HRR} - \dot{Q}_{loss}\right) - \frac{c_p}{c_v} \frac{p}{V_{cyl}} \dot{V}_{cyl} \tag{34}$$

4. Results and discussion

4.1. Simulation results of the multi-zone model

The Dual-fuel engine combustion model contains two parts, a multi-zone combustion model for the n-heptane and a flame propagation model for the ammonia. The multi-zone model determines the ignition delay of the overall combustion model. This, in turn, affects the subsequent flame propagation timing of the ammonia and, thus, the amount of ammonia fuel burned in an instant. Also, the multi-zone model contributes a portion of the overall heat release. In order to verify the effectiveness of the multi-zone model simulation, an experiment with n-heptane mono-fuel was carried out for the BUKH engine. The specific experimental operating parameters are listed in Table 4. The experimental cylinder pressure data were obtained, and the HRR was calculated. The n-heptane HRR curve and cylinder pressure were then simulated by the multi-zone model.

By observing the HRR in Fig. 4, the timing of the start of combustion (SOC) for the experimental and simulated curves fits well (SOC is determined to be at local minimum [41]), so the model has a good agreement on the ignition delay. The model also predicts generally well in terms of premixed combustion phases with crank angles of −5 to 5. However, at crank angles of 3–5°, it can be noticed that the HRR of the model is slightly higher than the experimental one. This is related to the fact that the evaporation rate of the simulated n-heptane droplets is somewhat faster than the actual one. In the subsequent mixing-controlled combustion phase, the simulated and experimental curves are in good agreement. The simulated cylinder pressure curve in Fig. 5 deviates somewhat from the experimental curve between crank angles 5 to 40. This is related to the misprediction of the specific heat parameters and the heat losses in the cylinder. (Obtained by model calibration and observation of parameters) Overall, the multi-zone model provides a good prediction of the combustion process for n-heptane.

4.2. Discussion of model and experimental results

This section contains four experiments with ammonia fuels at 80 %, 89 %, 95 % and 98 % energy proportions. The n-heptane and ammonia fuels were scaled by the level of energy contribution in the experiments. The energy proportion was varied by adjusting the injection flow rates of the n-heptane and ammonia fuels in the experiments. According to previous studies, the overall air/fuel equivalence ratio (λ) was kept constant in the experiment at 1.10 due to the high indicated efficiency at this λ value [13]. The start of injection (SOI) of 20 CAD BTDC was also chosen because of the high indicated efficiency of the engine at this

Table 4
Specific parameters for the BUKH engine operating n-heptane fuel.

RPM	Air/fuel equivalence ratio λ [−]	Charge air temperature T_{ch} [k]	Injection timing BTDC [deg]	Injection duration [deg]	Ignition Delay τ_{id} [deg]	Charge air pressure P_{ch} [bar]
1200	3.00	318	10	5.77	6.1	1.068

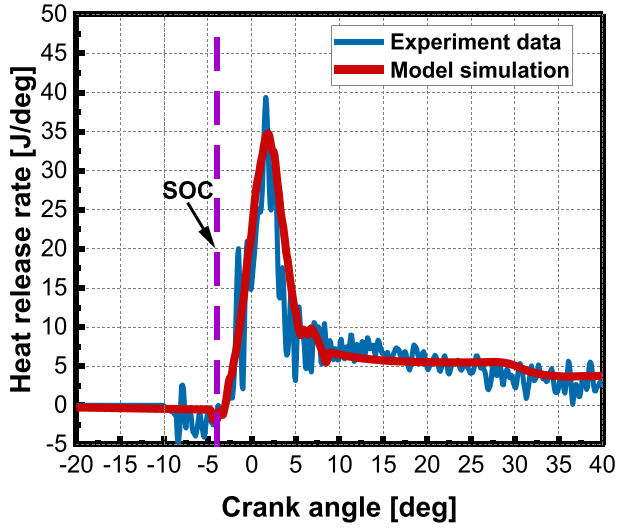

Fig. 4. Experimental HRR of n-heptane and HRR curve from multi-zone model simulation.

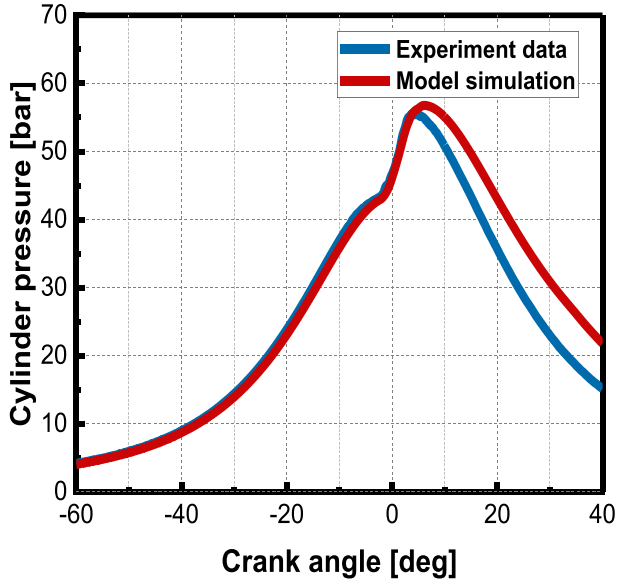

Fig. 5. Experimental cylinder pressure of n-heptane and cylinder pressure curve from multi-zone model simulation.

injection timing. In these cases, the combustion processes of ammonia fuel with different energy proportions were simulated and experimentally investigated. The specific engine operating parameters are listed in Table 5.

Fig. 6 illustrates the case of a 20 % proportion of n-heptane and an 80 % proportion of ammonia fuel. The experimental HRR (Fig. 6 (b)) shows a diesel-like combustion process. But in reality, this is a combined combustion process of dual fuel. There is a pronounced peak at the beginning of the experimental curve, followed by a mixing-controlled-like combustion process. The pronounced peek is most likely the result of pilot-fuel combustion. The subsequent heat release is caused by the flame propagation of the ignited ammonia fuel. In this case, the ammonia mixture has a λ of 1.38, which is a relatively lean mixture compared to the other cases. The leaner mixture has a slower flame speed (the highest flame speed is around 0.91 of the λ value) and therefore results in a slower rate of change in the volume of the ammonia mixture swept by the flame. This, in turn, leads to a lower HRR in the combustion phase of the ammonia fuel in this case compared to the other cases. Another reason could be that the higher amount of n-heptane is not beneficial to the combustion of the ammonia fuel.

From the simulated HRR, the simulated curve deviates somewhat from the experimental curve. The ignition delay is most noticeable, with the experimental ignition delay being 8.51 deg compared to the simulated ignition delay of 9.62 deg. The significant deviation in ignition delay results in a late simulated HRR peak for pilot fuel. The relatively large amount of n-heptane vapor accumulates during the ignition delay, resulting in a slightly larger peak for this simulation. Because of the late prediction of the ignition delay, the ammonia fuel is also ignited at a delayed time. This results in a large amount of delayed combustion of the ammonia fuel, so the simulated HRR in the 10–40 crank angle range is higher than the experimental HRR. The simulated cylinder pressure in Fig. 6 (a) is also higher than the experimental cylinder pressure, which is mainly due to the larger HRR predicted by the simulation (the simulated cylinder pressure is calculated from the simulated HRR) and the inaccurate prediction of the specific heat parameters.

From the experimental HRR in Fig. 7 (b) (89 % energy proportion of ammonia fuel), there is a clear peak at the beginning, as in the case of 80 % ammonia fuel energy. Here it is still considered to be resulting from n-heptane combustion. However, this peak is relatively low due to the reduction of the n-heptane energy proportion from 20 % to 11 % in this case. The other reason is that the ignition delay is slightly shorter in this case, so less n-heptane vapor accumulates in this period, resulting in a lower peak. The subsequent phase is the HRR of ammonia fuel combustion, where the HRR values are higher than in the 80 % case. This is mainly due to the increased energy proportion of ammonia fuel. In addition, because the λ of the ammonia mixture is 1.25 in this case, the flame propagation speed is higher than in the 80 % case (λ is 1.38). Therefore, the burning amount of the ammonia fuel in the same time span is increased, which also leads to a higher HRR.

Table 5
Specific parameters for the BUKH engine operating n-heptane/ammonia dual-fuel.

Ammonia energy proportions [%]	Air/fuel equivalence ratio (ammonia) λ_{NH_3} [−]	Air/fuel equivalence ratio (overall) λ [−]	Charge ammonia mixture temperature T_{ch} [k]	Injection timing BTDC [deg]	Injection duration [ms]	Ignition Delay τ_{id} [deg]	Charge air pressure P_{ch} [bar]	RPM	Total fuel energy [J]
80	1.38	1.10	353	20	0.43	8.51	1.225	1200	1290
89	1.25	1.10	353	20	0.25	8.09	1.201	1200	1203
95	1.16	1.10	353	20	0.16	8.77	1.204	1200	1190
98	1.11	1.10	353	20	0.09	10.02	1.208	1200	1205

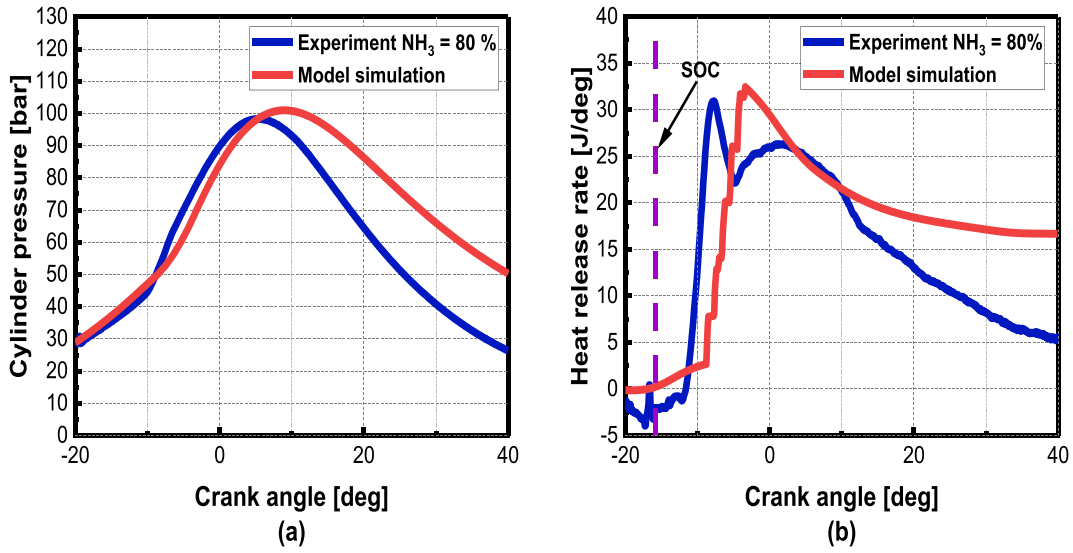

Fig. 6. (a) Simulated and experimental cylinder pressure curves and (b) Simulated and experimental heat release rate curves under the condition of energy proportion of 80 % for NH_3.

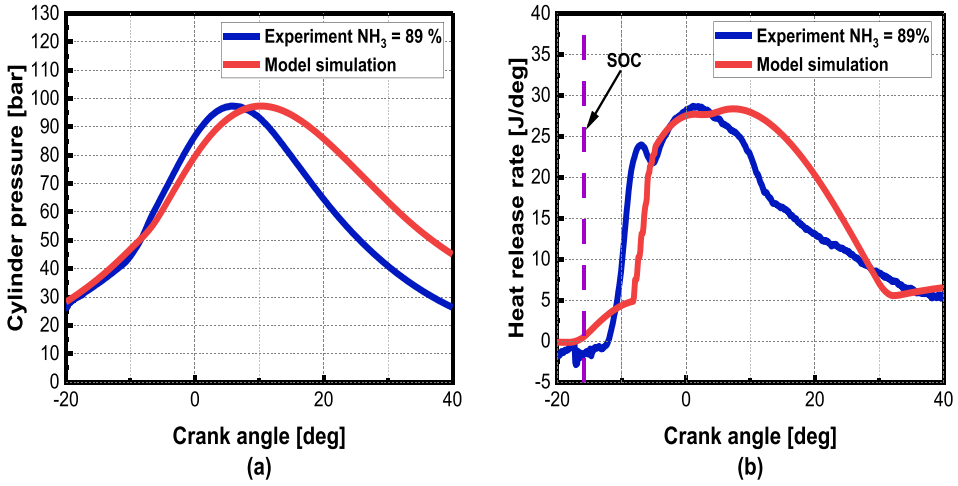

Fig. 7. (a) Simulated and experimental cylinder pressure curves and (b) Simulated and experimental heat release rate curves under the condition of energy proportion of 89 % for NH_3.

The simulated HRR in Fig. 7 (b) has a slight deviation in ignition delay from the experimental one, which is less than the deviation for the 80 % ammonia fuel case. From the simulated HRR, an insignificant peak of n-heptane combustion can be seen (lasting until about 4° of crank angle). The simulated HRR of the subsequent combustion phase of the ammonia fuel is higher than the experimental HRR. One reason is the ignition delay deviation, so the ammonia fuel is burned later. The other reason could be that the simulated flame speed of the ammonia mixture is too fast. Thus, more simulated ammonia fuel burns quickly, resulting in a high HRR. The cylinder pressure deviation in Fig. 7(a) is for the same reason as in the 80 % ammonia fuel case and will not be repeated here.

Fig. 8 shows the case of combustion with a 5 % energy proportion of n-heptane and a 95 % energy proportion of ammonia fuel. As can be seen from the experimental HRR in Fig. 8 (b), a small peak of n-heptane combustion can be observed in the range of approximately −7° of crank angles (due to the small energy proportion of n-heptane), followed by the combustion of the ammonia fuel. There are three reasons for the higher HRR of the ammonia mixture in this case compared to the 80 % and 89 % ammonia fuel cases. The first reason is the large energy proportion of the ammonia fuel in this case, i.e., 95 % of the ammonia fuel. The second reason is that the flame propagation is faster at this λ value (1.16) compared to the previous two cases, so more ammonia fuel combusts in the same time-lapse. The last reason could be that the λ value is further reduced in this case (richer mixture) compared to the previous two cases, and the richer ammonia mixture is more favorable for ammonia combustion and thus have a higher HRR for the ammonia phase.

From the simulated HRR of Fig. 8 (b), there is a small deviation between the simulated HRR and the experimental one, so the overall simulated HRR fits well. The simulated HRR is slightly higher than the experimental HRR from 3 to 18°, for the same reason as the previous two cases, because of the ignition delay deviation. From 18 to 40°, the simulated HRR is lower than the experimental one. One reason for this is that the simulated turbulent flame speed may be slower than the actual flame speed. The second reason is that the simulated heat loss is larger than the actual heat loss, so the simulated HRR is too low. Overall, however, the simulated HRR, in this case, has a small deviation. Fig. 8 (a) shows a lesser deviation in-cylinder pressure than the previous two cases for the same reason and will not be repeated here.

Fig. 9 shows the last case, i.e., 2 % energy proportion n-heptane and 98 % energy proportion ammonia fuel. From the experimental HRR,

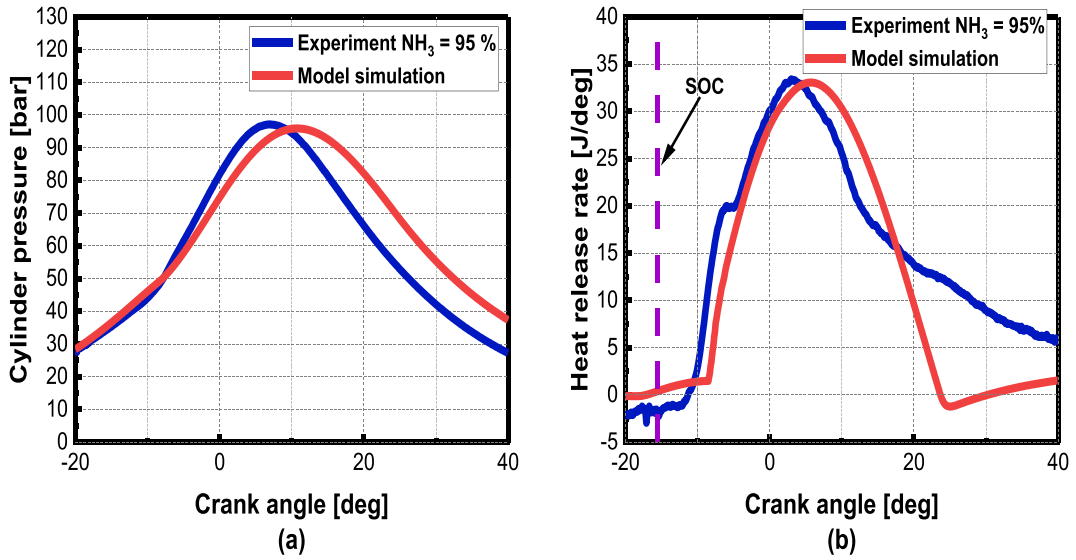

Fig. 8. (a) Simulated and experimental cylinder pressure curves and (b) Simulated and experimental heat release rate curves under the condition of energy proportion of 95 % for NH_3.

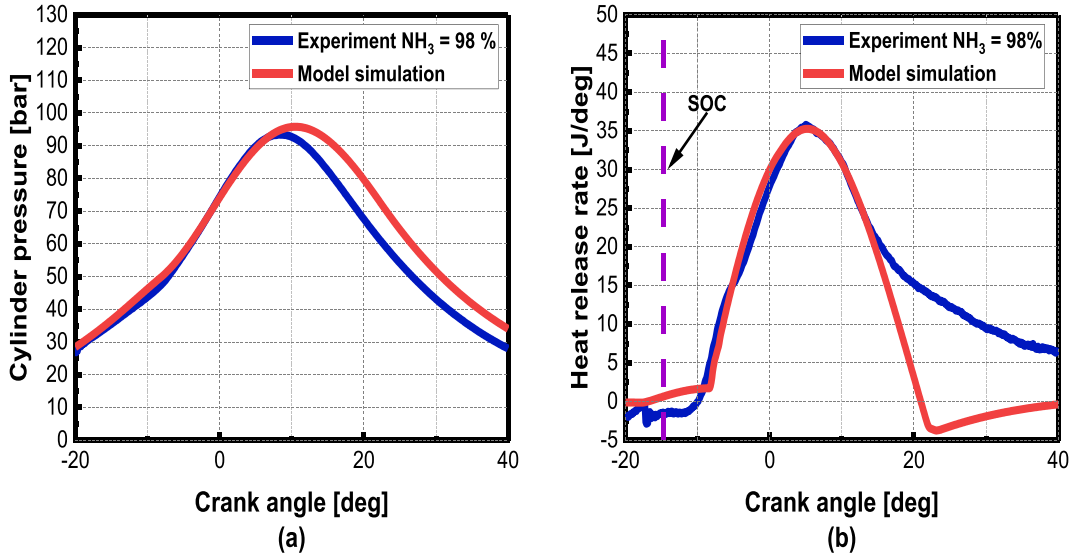

Fig. 9. (a) Simulated and experimental cylinder pressure curves and (b) Simulated and experimental heat release rate curves under the condition of energy proportion of 98 % for NH_3.

there is a quite insignificant peak at a crank angle of −6°, most likely due to the combustion of the n-heptane. After that, it goes to the HRR phase of the ammonia fuel. The ammonia fuel phase, in this case, has the highest HRR. The reasons for this high HRR are the same as in the 95 % ammonia proportion case. That is, the high proportion of ammonia energy, the fast flame propagation speed (at the current λ value of 1.11), and in this case, the richer ammonia mixture will be more favorable for its combustion. The above reasons lead to the highest ammonia HRR in this case.

The simulated HRR of Fig. 9 (b) shows that it has only a slight deviation from the experimental ignition delay. So, the overall simulated HRR and the experimental HRR are in good agreement. However, in the 15–40 crank angle range, the simulated HRR is lower than the experimental HRR. Probably because the simulated flame propagation speed is too slow, and the predicted Woschni heat transfer loss is larger than the actual value, as in the previous case. As can be observed from Fig. 9 (a), because of the slight HRR deviation, the cylinder pressure deviation for the simulation, in this case, is also small.

By observing these four cases, the experimental HRR for each case consists of an n-heptane combustion peak and a subsequent ammonia combustion phase. As the energy proportion of the ammonia fuel increases, the HRR values for its combustion phase become larger and larger. This is closely related to the energy proportion of the ammonia fuel, the flame propagation speed, and the richness or leanness of the ammonia mixture. In terms of the simulated HRR, as the ammonia fuel proportion increases, the ignition delay deviation between the experimental and simulated HRR becomes smaller, and the overall HRR simulation becomes better. In addition, there is always a certain deviation of cylinder pressure between experimental and simulated, but this deviation also becomes smaller and smaller as the ammonia fuel proportion increases. The main reason is that the decreasing deviation in simulation HRR leads to the decreasing deviation in cylinder pressure.

4.3. Discussion and analysis of ignition delay

Fig. 10 illustrates that the experimental and simulated ignition

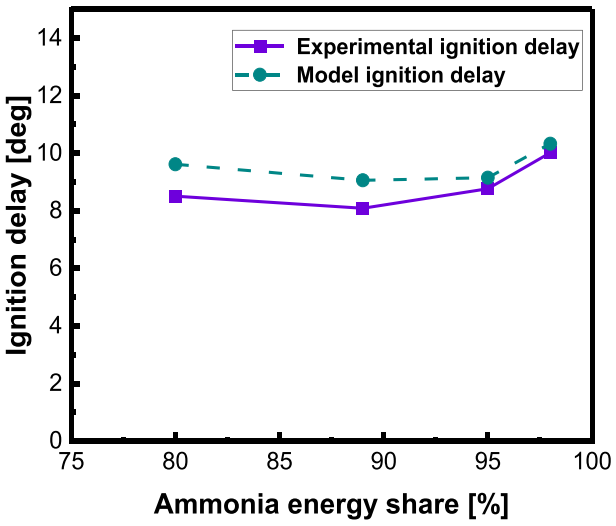

Fig. 10. Experimental and simulated total ignition delay for different cases of ammonia fuel energy proportion.

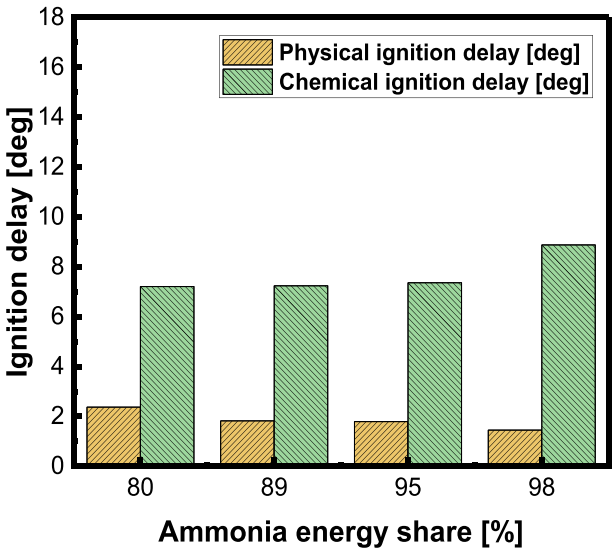

Fig. 11. Simulated physical and chemical ignition delay for different cases of ammonia fuel energy proportion.

delays show the same trend. As a whole, increasing the energy proportion of ammonia fuel increases the ignition delay (there is a slight decrease in the ignition delay for the 89 % ammonia energy proportion case). It is believed here that increasing the proportion of ammonia prevented the oxidation process of n-heptane, thus increasing the ignition delay. It is also possible to consider the cetane number of the two fuels, which is an important parameter to measure the ignition performance of a fuel. The higher the cetane number, the better the ignition performance. N-heptane has a cetane number of approximately 56, while the cetane number of ammonia fuel is negligible [42,43]. When the energy proportion of ammonia fuel increases, a higher proportion of ammonia is mixed with n-heptane, which leads to a lower cetane number in the overall mixture, resulting in a longer ignition delay. From the ignition delay simulation results for these four cases, the deviations for the 80 % and 89 % ammonia fuel cases are more significant than those for the 95 % and 98 % cases. This is likely to be related to deviations in the evaporation of the n-heptane from the multi-zone simulations, resulting in a deviation in the fuel/air equivalence ratio from the actual value (Equation (14)) and hence the eventual ignition delay deviation.

Physical ignition delay refers to the period by which the n-heptane is injected from the injector, and undergoes break-up, atomization, evaporation and mixing with the ammonia mixture in the cylinder [44,45]. Chemical ignition delay refers to the period between the chemical decomposition of n-heptane and the rapid chemical reaction leading to combustion. Typically, the chemical ignition delay is longer than the physical ignition delay. As can be observed in Fig. 11, the physical ignition delay in all four cases decreases as the proportion of ammonia fuel energy increases. This is because the ammonia fuel mixture inhaled into the cylinder is at a higher temperature of 353 K. As the ammonia fuel energy proportion increases, the temperature inside the cylinder also rises simultaneously. The higher the cylinder temperature, the better the n-heptane atomization, evaporation, and mixing process, so the physical ignition delay tends to be shorter. The chemical ignition delay shows that in the 80 % and 89 % ammonia energy proportion cases, it remains more or less the same. In the 95 % case, there is a slight increase, and in the 98 % case, there is a significant increment. This is due to the poor ignition performance of the ammonia fuel affecting the ignition capacity of the n-heptane and ammonia fuel mixture. According to Hardenberg and Hase's formula, the activation energy of ammonia fuel is 27,273 J/mol while the activation energy of n-heptane is 8417 J/mol (higher activation energy means that more energy is required to enable the fuel to ignite, and thus the chemical ignition delay is longer) [46]. As the proportion of ammonia energy increases, more ammonia fuel is mixed into the n-heptane mixture, so the activation energy of the blend as a whole is higher, and therefore the chemical ignition delay is more prolonged. This is particularly evident in the 98 % ammonia case. It is also clear from the four cases that the chemical ignition delay is always significantly longer than the physical one.

4.4. Discussion and analysis of indicated efficiencies

Fig. 12 presents the indicated efficiencies for the experiments and simulations for the four cases. The experimental indicated efficiencies show that as the proportion of ammonia fuel energy increases, the indicated efficiency also increases. This can be explained by the CA50 in Fig. 13, which reflects the share of heat released from the fuel on the utilization of the engine compression ratio. The earlier the CA50, the greater the share of the heat energy utilized by the engine compression ratio. The later the CA50, the smaller the share of the heat energy utilized by the engine compression ratio, which reduces the part of the

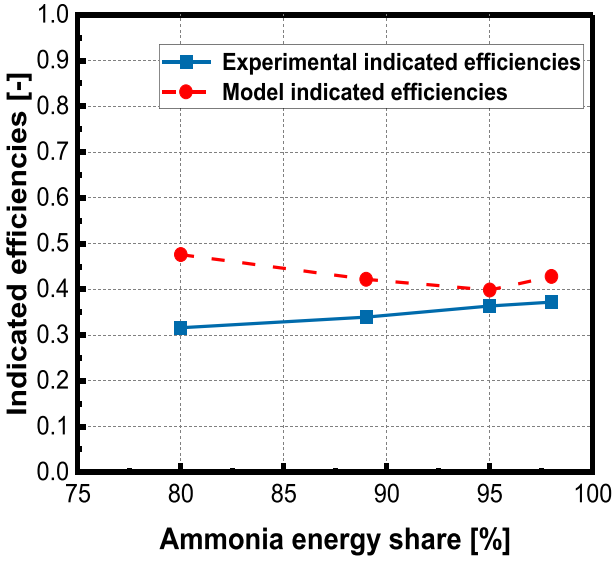

Fig. 12. Experimental and simulated indicated efficiencies for different cases of ammonia fuel energy proportion.

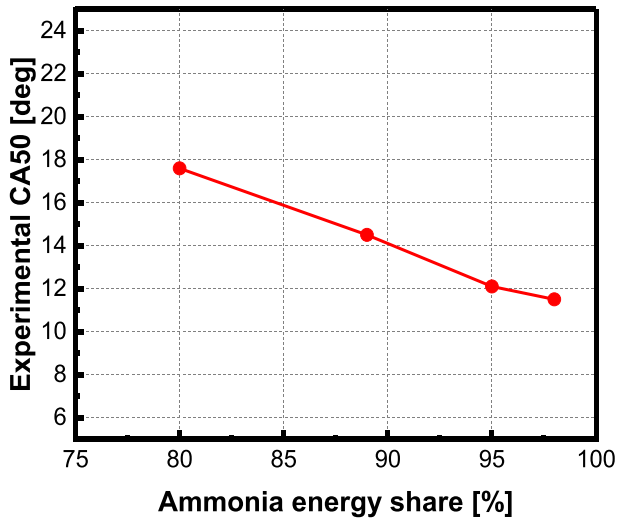

Fig. 13. Experimental CA50 for different cases of ammonia fuel energy proportion.

cylinder expansion converted from heat to work, thus reducing the indicated efficiency [47,48]. CA50 is also highly sensitive to the heat loss of the cylinder. The later the CA50, the higher the heat loss of the cylinder [49].

The 80 % ammonia fuel case in Fig. 13 has the latest CA50, followed by the 89 % case and then the 95 % case, with the earliest CA50 being the 98 % case. So the 80 % ammonia fuel case has the lowest indicated efficiency, and the 89 %, 95 %, and 98 % ammonia fuel cases have progressively higher indicated efficiencies. The simulated 80 % ammonia case in Fig. 12 has a certain deviation compared to the experimental case. This is due to the cylinder pressure deviation caused by the HRR and ignition delay deviation in this case and, therefore, the eventual deviation in the indicated efficiency. 89 %, 95 %, and 98 % ammonia cases have less significant deviations in the indicated efficiency also due to the cylinder pressure deviation. From the analysis of the simulation results, it can be concluded that if the simulated ignition delay and HRR fit the experimental data better, the better the simulated cylinder pressure fits the experimental data, which ultimately leads to a smaller deviation in the simulated indicated efficiency. In Fig. 12, the curve trend of the indicated efficiency of the experiment is increasing, while the curve trend of the simulation is decreasing and then increasing. This is due to the deviation of the simulated indicated efficiencies for the 80 % and 89 % ammonia fuel cases, where the simulated ignition delays and HRRs are somewhat deviating from the experimental results, which leads to deviation in the simulated cylinder pressures. The deviations in the simulated cylinder pressures then lead to deviations in the simulated indicated efficiencies (the indicated efficiencies were calculated based on cylinder pressures and cylinder volume changes), thus changing the trend of the curve.

Nomenclature

A	Ignition delay parameter (−) Area (m^2)
a, c	Constant coefficients (−)
B	Injected fuel volume per cycle (m^3)
B_{cyl}	Cylinder bore (m)
c_0	Air entrainment tuning coefficient (−)
c_p	Specific heat at constant pressure ($J/kg \bullet K$)
c_v	Specific heat at constant volume ($J/kg \bullet K$)
c_{mix}	Air entrainment tuning coefficient (−)
D	Sauter Mean Diameter (μm)
DB	Mass diffusivity (m^2/s)

5. Conclusion

This work investigated the light-duty BUKH compression-ignition engine with n-heptane as the pilot fuel and ammonia as the primary fuel through experimental and simulation methods. The multi-zone combustion model for n-heptane and the flame propagation model for ammonia fuel were developed based on the summary of the previous research. The multi-zone model has been calibrated by means of experimental cases with n-heptane fuel. Experiments with n-heptane and ammonia fuels of different energy proportions were carried out on the BUKH engine. The experimental data were then compared with the model results, and the overall model was then calibrated. The experimental and simulated HRR, cylinder pressure, ignition delay, and indicated efficiencies were analyzed and discussed in detail.

1. In this work, it was found that the combustion process of a dual-fuel engine can be simulated by combining a multi-zone model for n-heptane and a flame propagation model for ammonia fuel. Among them, the evaporative combustion multi-zone model of pilot fuel is quite accurate in conducting model validation. It was found that the higher the proportion of ammonia fuel, the lower the simulation deviation of heat release rate and cylinder pressure. For example, the simulation results for the case with 98 % ammonia fuel energy ratio are better than the case with 80 % ammonia fuel energy ratio. The critical reason for this result is related to the accuracy of the prediction of the mass burn rate of ammonia fuel.
2. This work found that the lesser the difference between the simulated and experimental ignition delay, the better the simulation of heat release rate and cylinder pressure. In the four cases of 80 %, 89 %, 95 % and 98 % ammonia fuel energy ratio, the deviations of the simulated ignition delay to the experimental ignition delay are 1.11, 0.97, 0.38, and 0.31, respectively. The decrease in the ignition delay deviation resulted in the reduction of the deviation in the simulated heat release rate and cylinder pressure. This was because the lower ignition delay deviation ensured the proper prediction of the ammonia fuel mass burning rate, which led to the reduction of the deviation. It was also found that the chemical ignition delay of n-heptane is always much longer than the physical ignition delay. If the ignition performance of n-heptane is intended to be improved, its chemical ignition delay should be the priority.
3. Several reasons that lead to deviations in simulations and experiments were found. These factors included ignition delay, heat losses, specific heat parameters, and flame speed, which offered a hint for future modelling improvements.

Declaration of competing interest

The authors declare that they have no known competing financial interests or personal relationships that could have appeared to influence the work reported in this paper.

d	Diameter (m)
D_{AB}	Binary diffusion coefficient (m^2/s)
E_t	Activation temperature (K)
f_f	Flame coefficient of turbulence (−)
h	Enthalpy (J/kg)
h_w	Heat transfer coefficient ($W/m^2 \bullet K$)
k	Thermal conductivity ($W/m \bullet K$)
m	Mass (kg)
n	Amount of substance (mol)
Nu	Nusselt number (−)
Pr	Prandtl number (−)
p	Pressure (Pa)
Q	Heat transfer (J)
R	Molar gas constant ($J/mol \bullet K$)
Re	Reynolds number (−)
R_f	Flame radius (m)
S	Penetration length (m)
s_1, s_2	Fitting parameters (−)
Sh	Sherwood number (−)
Sc	Schmidt number (−)
T	Temperature (K)
t	Time (s)
u	Specific internal energy (J/kg)
v	Velocity (m/s)
V	Volume (m^3)
w	Characteristic velocity (m/s)
z	Correction factor (−)
Δh	Latent heat (J/kg)

Greek symbols

α	Temperature exponent (−)
γ	Pressure exponent (−)
θ	Initial spray angle (radian)
θ	Crank angle position (radian)
κ, β	Ignition delay parameters (−)
λ	Air/fuel equivalence ratio (−)
μ	Dynamic viscosity ($N \bullet s/m^2$)
ρ	Density (kg/m^3)
τ	Ignition delay (s)
$\varnothing$	Fuel/air equivalence ratio (−)

Subscripts

a	Air
am	Ammonia-air mixture
ammo	Ammonia
b	Burning zone
bu	Breakup
cyl	Cylinder
con	Consumed fuel
d	Droplet
diff	Diffusion combustion
evap	Evaporation
Entr	Entrained air
f	Fuel
f_f	Flame coefficient of turbulence (−)
fl	Flame
FP	Fuel packets
g	Gas phase
HR	Heat release
HRR	Heat release rate
inj	Injection
i	Heat loss parts
id	Ignition delay
j	Axial packet index
k	Radial packet index

l	Laminar
loss	Heat loss
max	Maximum
N	Total number of heat loss parts
n	n-heptane
noz	Nozzle
p	Piston
p	Premixed combustion
ref	Reference state
s	Surface conditions
sat	Saturation condition
stoic	Stoichiometric
t	Turbulent
u	Unburned zone
v	Vapor phase
0	Initial state

Abbreviation

AF	Air-fuel ratio
ATDC	After top dead center
BP	Burning packet
BTDC	Before top dead center
CA	Crank angle
CA50	Crank angle at 50 % completion of heat release
CI	Compression ignition
COV	Coefficient of variation
CR	Compression ratio
HRR	Heat release rate
ICE	Internal combustion engine
LHV	Lower heating value
RPM	Revolutions per minute
SI	Spark-ignition
SOC	Start of combustion
SOI	Start of injection
SP	Spray penetration

References

[1] Chiong MC, Chong CT, Ng JH, Mashruk S, Chong WWF, Samiran NA, Mong GR, Valera-Medina A. Advancements of combustion technologies in the ammonia-fuelled engines. Energy Convers Manag 2021;244:114460. https://doi.org/10.1016/j.enconman.2021.114460.

[2] Chu H, Ya Y, Nie X, Qiao F, E J. Effects of adding cyclohexane, n-hexane, ethanol, and 2,5-dimethylfuran to fuel on soot formation in laminar coflow n-heptane/iso-octane diffusion flame, Combust. Flame 2021;225:120–35. https://doi.org/10.1016/j.combustflame.2020.10.030.

[3] Liu L, Wu Y, Wang Y. Numerical investigation on the combustion and emission characteristics of ammonia in a low-speed two-stroke marine engine. Fuel 2022;314:122727. https://doi.org/10.1016/j.fuel.2021.122727.

[4] Scherban AV. The greenhouse effect and its impacts on environment. Econ. Ecol. Territ. Educ. 2021;5:59–65. https://doi.org/10.23947/2413-1474-2021-5-2-59-65.

[5] Liobikienė G, Butkus M. The European Union possibilities to achieve targets of Europe 2020 and Paris agreement climate policy. Renew Energy 2017;106:298–309. https://doi.org/10.1016/j.renene.2017.01.036.

[6] Nadimi E, Przybyła G, Emberson D, Løvås T, Ziółkowski Ł, Adamczyk W. Effects of using ammonia as a primary fuel on engine performance and emissions in an ammonia/biodiesel dual-fuel CI engine. Int J Energy Res 2022;46:15347–61. https://doi.org/10.1002/er.8235.

[7] Schramm J, Klüssmann JN, Ekknud LR, Ivarsson A. Ammonia application in IC engines. Adv. Mot. Fuels Technol. Collab. Program. 2020 4-4.

[8] Stiesch G, Merker GP. A phenomenological model for accurate and time efficient prediction of heat release and exhaust emissions in direct-injection diesel engines. SAE Tech. Pap. 1999. https://doi.org/10.4271/1999-01-1535.

[9] Papagiannakis RG, Hountalas DT, Kotsiopoulos PN. Experimental and theoretical analysis of the combustion and pollutants formation mechanisms in dual fuel di diesel engines. SAE Tech. Pap. 2005. https://doi.org/10.4271/2005-01-1726.

[10] Nadimi E, Przybyła G, Lewandowski MT, Adamczyk W. Effects of ammonia on combustion, emissions, and performance of the ammonia/diesel dual-fuel compression ignition engine. J Energy Inst 2023;107. https://doi.org/10.1016/j.joei.2022.101158.

[11] Yousefi A, Guo H, Dev S, Lafrance S, Liko B. A study on split diesel injection on thermal efficiency and emissions of an ammonia/diesel dual-fuel engine. Fuel 2022;316:123412. https://doi.org/10.1016/j.fuel.2022.123412.

[12] Mi S, Wu H, Pei X, Liu C, Zheng L, Zhao W, Qian Y, Lu X. Potential of ammonia energy fraction and diesel pilot-injection strategy on improving combustion and emission performance in an ammonia-diesel dual fuel engine. Fuel 2023;343:127889. https://doi.org/10.1016/j.fuel.2023.127889.

[13] Førby N, Thomsen TB, Cordtz RF, Bræstrup F, Schramm J. Ignition and combustion study of premixed ammonia using GDI pilot injection in CI engine. Fuel 2023;331:125768. https://doi.org/10.1016/j.fuel.2022.125768.

[14] Frigo S, Gentili R. Analysis of the behaviour of a 4-stroke Si engine fuelled with ammonia and hydrogen. Int J Hydrogen Energy 2013;38:1607–15. https://doi.org/10.1016/j.ijhydene.2012.10.114.

[15] Ryu K, Zacharakis-Jutz GE, Kong SC. Performance enhancement of ammonia-fueled engine by using dissociation catalyst for hydrogen generation. Int J Hydrogen Energy 2014;39:2390–8. https://doi.org/10.1016/j.ijhydene.2013.11.098.

[16] Mørch CS, Bjerre A, Gøttrup MP, Sorenson SC, Schramm J. Ammonia/hydrogen mixtures in an SI-engine: engine performance and analysis of a proposed fuel system. Fuel 2011;90:854–64. https://doi.org/10.1016/j.fuel.2010.09.042.

[17] Westlye FR, Ivarsson A, Schramm J. Experimental investigation of nitrogen based emissions from an ammonia fueled SI-engine. Fuel 2013;111:239–47. https://doi.org/10.1016/j.fuel.2013.03.055.

[18] Dinesh MH, Pandey JK, Kumar GN. Study of performance, combustion, and NOx emission behavior of an SI engine fuelled with ammonia/hydrogen blends at various compression ratio. Int J Hydrogen Energy 2022;47:25391–403. https://doi.org/10.1016/j.ijhydene.2022.05.287.

[19] W.M. Haynes, CRC handbook of chemistry and physics, n.d.

[20] Ratcliff MA, Mccormick RL, Taylor JD. Compendium of experimental cetane numbers compendium of experimental cetane numbers. 2017.

[21] Nie X, Qi J, Feng S, Liu Y, Qiu B, Chu H. Soot formation in n-heptane/air laminar diffusion flames: effect of toluene addition, Fuel Process. Technol 2022;234:107324. https://doi.org/10.1016/j.fuproc.2022.107324.

[22] Chu H, Xiang L, Nie X, Ya Y, Gu M, Jiaqiang E. Laminar burning velocity and pollutant emissions of the gasoline components and its surrogate fuels: a review. Fuel 2020;269:117451. https://doi.org/10.1016/j.fuel.2020.117451.

[23] Hiroyuki Hiroyasu TK. Development and use of a spray combustion modeling to predict diesel engine efficiency and pollutant emissions. Chem Pharm Bull 1983; 40:1569–72.
[24] Hiroyuki Hiroyasu TK. Development and use of a spray combustion modeling to predict diesel engine efficiency and pollutant emissions. Chem Pharm Bull 2002: 2091. http://www.mendeley.com/research/geology-volcanic-history-eruptive-style-yakedake-volcano-group-central-japan/.
[25] Bazari Z. A di diesel combustion and emission predictive capability for use in cycle simulation. SAE Tech. Pap. 1992;101:747–70. https://doi.org/10.4271/920462.
[26] Gao Z, Schreiber W. The effects of EGR and split fuel injection on diesel engine emission. Int J Automot Technol 2001;2:123–33.
[27] Kouremenos DA, Rakopoulos CD, Hountalas DT. Multi-zone combustion modelling for the prediction of pollutants emissions and performance of di diesel engines. SAE Tech. Pap. 1997;106:940–57. https://doi.org/10.4271/970635.
[28] Stiesch G. Modeling engine spray and combustion processes. 2004. https://doi.org/10.2514/1.14200.
[29] Hountalas DT, Papagiannakis RG. Development of a simulation model for direct injection dual fuel diesel-natural gas engines. SAE Tech. Pap. 2000;109:373–83. https://doi.org/10.4271/2000-01-0286.
[30] Cheng C, Cordtz RF, Thomsen TB, Schramm J. Application of methanol with an ignition improver in a small marine CI engine. Energy Convers Manag 2022;271: 1–14. https://doi.org/10.1016/j.enconman.2022.116311.
[31] Histories UV. Unsteady vaporization histories and trajectories of fuel drops injected into swirling air unsteady vaporization histories and trajectories of fuel drops. 1962.
[32] Hountalas DT, Papagiannakis RG. Theoretical and experimental investigation of a direct injection dual fuel diesel-natural gas engine. SAE Tech. Pap. 2002. https://doi.org/10.4271/2002-01-0868.
[33] Metghalchi M, Keck JC. Burning velocities of mixtures of air with methanol, isooctane, and indolene at high pressure and temperature. Combust Flame 1982; 48:191–210. https://doi.org/10.1016/0010-2180(82)90127-4.
[34] Takizawa K, Takahashi A, Tokuhashi K, Kondo S, Sekiya A. Burning velocity measurements of nitrogen-containing compounds. J Hazard Mater 2008;155: 144–52. https://doi.org/10.1016/j.jhazmat.2007.11.089.
[35] Ghanaati A, Mat Darus IZ, Muhamad Said MF, Mahmoudzadeh Andwari A. A mean value model for estimation of laminar and turbulent flame speed in spark-ignition engine. Int J Automot Mech Eng 2015;11:2224–34. https://doi.org/10.15282/ijame.11.2015.5.0186.
[36] Lipatnikov AN, Li WY, Jiang LJ, Shy SS. Does density ratio significantly affect turbulent flame speed?, flow. Turbul. Combust. 2017;98:1153–72. https://doi.org/10.1007/s10494-017-9801-6.
[37] Ratzke A, Schöffler T, Kuppa K, Dinkelacker F. Validation of turbulent flame speed models for methane-air-mixtures at high pressure gas engine conditions. Combust Flame 2015;162:2778–87. https://doi.org/10.1016/.j.combustflame.2015.04.011.
[38] Hountalas DT, Papagiannakis RG. A simulation model for the combustion process of natural gas engines with pilot diesel fuel as an ignition source. SAE Tech. Pap. 2001;110:1496–509. https://doi.org/10.4271/2001-01-1245.
[39] Wang H, DelVescovo D, Reitz RD, Yao M. Numerical study of RCCI and HCCI combustion processes using gasoline, diesel, iso-butanol and DTBP cetane improver. SAE Int. J. Engines. 2015;8:831–45. https://doi.org/10.4271/2015-01-0850.
[40] Sorenson SC. Internal combustion engine principles. ISBN 8792130577, 978-8792130570 1985;76.
[41] Finesso R, Spessa E. Ignition delay prediction of multiple injections in diesel engines. Fuel 2014;119:170–90. https://doi.org/10.1016/j.fuel.2013.11.040.
[42] Nguyen DK, Le AT, Thi THT, Wu MH. A 1-D numerical analysis on the control of HCCI combustion in a CI engine through exhaust gas recirculation. J. Chinese Soc. Mech. Eng. Trans. Chinese Inst. Eng. Ser. C/Chung-Kuo Chi Hsueh K. Ch'eng Hsuebo Pao. 2018;39:179–86.
[43] Gray JT, Dimitroff E, Meckel NT, Quillian RD. Ammonia fuel - engine compatibility and combustion. SAE Tech. Pap. 1966;75:785–807. https://doi.org/10.4271/660156.
[44] Pedersen PS, Qvale B. A model for the physical part of the ignition delay in a diesel engine. SAE Tech. Pap. 1974;83:2625–38. https://doi.org/10.4271/740716.
[45] Rosseel E. The physical and the chemical part of the ignition delay in diesel engines. SAE Tech. Pap 1996;12:3–5. https://doi.org/10.4271/961123.
[46] Duong MQ, Nguyen VH, Pham PX. Development of empirical correlations for ignition delay in a single cylinder engine fueled with diesel/biodiesel blends. Proc. 2019 Int. Conf. Syst. Sci. Eng. ICSSE 2019;2019:614–8. https://doi.org/10.1109/ICSSE.2019.8823131.
[47] Cheng C, Cordtz RF, Pedersen TD, Winther K, Førby NL, Schramm J. Investigation of combustion characteristics, physical and chemical ignition delay of methanol fuel in a heavy-duty turbo-charged compression ignition engine. Fuel 2022;348. https://doi.org/10.2139/ssrn.4313214.
[48] Klimstra J. The optimum combustion phasing angle-A convenient engine tuning criterion. SAE Tech. Pap. 1985;94:602–10. https://doi.org/10.4271/852090.
[49] Carvalho L De O, De Melo TCC, De Azevedo Cruz Neto RM. Investigation on the fuel and engine parameters that affect the half mass fraction burned (CA50) optimum crank angle. SAE Tech. Pap. 2012. https://doi.org/10.4271/2012-36-0498.